



Delft University of Technology

Sensitivity Analysis and Parameterization of Gridded and Lumped Models Representation for Heterogeneous Land Use and Land Cover

Pudasaini, Prakash ; Assumpção, Thaine H.; Jonoski, Andreja; Popescu, Ioana

DOI

[10.3390/w16182608](https://doi.org/10.3390/w16182608)

Publication date

2024

Document Version

Final published version

Published in

Water

Citation (APA)

Pudasaini, P., Assumpção, T. H., Jonoski, A., & Popescu, I. (2024). Sensitivity Analysis and Parameterization of Gridded and Lumped Models Representation for Heterogeneous Land Use and Land Cover. *Water*, 16(18), Article 2608. <https://doi.org/10.3390/w16182608>

Important note

To cite this publication, please use the final published version (if applicable). Please check the document version above.

Copyright

Other than for strictly personal use, it is not permitted to download, forward or distribute the text or part of it, without the consent of the author(s) and/or copyright holder(s), unless the work is under an open content license such as Creative Commons.

Takedown policy

Please contact us and provide details if you believe this document breaches copyrights. We will remove access to the work immediately and investigate your claim.

Article

Sensitivity Analysis and Parameterization of Gridded and Lumped Models Representation for Heterogeneous Land Use and Land Cover

Prakash Pudasaini ¹, Thaine H. Assumpção ^{2,3} , Andreja Jonoski ²  and Ioana Popescu ^{2,3,*} ¹ Department of Water Resources and Irrigation, Kathmandou 44600, Nepal; ppudasaini086@gmail.com² Department of Hydroinformatics and Socio-Technical Innovation, IHE Delft, 2611 AX Delft, The Netherlands; t.hermanassumpcao@un-ihe.org (T.H.A.); a.jonoski@un-ihe.org (A.J.)³ Faculty of Civil Engineering and Geosciences, Delft University of Technology, 2628 CN Delft, The Netherlands

* Correspondence: i.popescu@un-ihe.org

Abstract: Hydrological processes can be highly influenced by changes in land use land cover (LULC), which can make hydrological modelling also very sensitive to land cover characterization. Therefore, obtaining up-to-date LULC data is a crucial process in hydrological modelling, and as such, different sources of LULC data raises questions on their quality and applicability. This is especially true with new data sources, such as citizen science-based land cover maps. Therefore, this research aims to explore the influence of LULC data sources on hydrological models via their parameterization and by performing sensitivity analyses. Kifissos catchment, in Greece, a poorly gauged and highly urbanized basin including the city of Athens, is the case study area. In total, 12 continuous hydrological models were developed by mainly varying their structure and parametrization (lumped and gridded) and using three LULC datasets: coordination of information on the environment (CORINE), Urban Atlas and Scent (citizen-based). It was found that excess precipitation is negligibly contributed to by soil saturation and is dominated by the runoff over impervious areas. Therefore, imperviousness was the main parameter influencing both sensitivity to land cover and parameterization. Lastly, although the parametrization as lumped and gridded models affected the representation of hydrological processes in pervious areas, it was not relevant in terms of excess precipitation.

Keywords: land use land cover; HEC-HMS; CORINE; urban atlas; scent; kifissos; hydrological model; parameterization; sensitivity



Citation: Pudasaini, P.; Assumpção, T.H.; Jonoski, A.; Popescu, I. Sensitivity Analysis and Parameterization of Gridded and Lumped Models Representation for Heterogeneous Land Use and Land Cover. *Water* **2024**, *16*, 2608. <https://doi.org/10.3390/w16182608>

Academic Editor: Bommana Krishnappan

Received: 14 August 2024

Revised: 10 September 2024

Accepted: 11 September 2024

Published: 14 September 2024



Copyright: © 2024 by the authors. Licensee MDPI, Basel, Switzerland. This article is an open access article distributed under the terms and conditions of the Creative Commons Attribution (CC BY) license (<https://creativecommons.org/licenses/by/4.0/>).

1. Introduction

The hydrological cycle is influenced by several factors, such as type of soil, land use and land cover and climatic and weather conditions. Specifically, land cover and climate variability are important features affecting hydrological processes, causing significant changes to overland flow and evapotranspiration [1,2]. Increased overland flow can be linked to an increase in floods, as the main reasons behind the increase in flood events (i.e., from around 100 in 1980 to 321 in 2010 in Europe [3]) are population growth, climate change and human activities such as deforestation and change in land use patterns. Urbanization, generally also linked to flash floods, is also increasing over the globe, from 30% of urbanized areas in 1950 to 55% in 2018 [4], while in 2010 75% of Europe was considered urban [5]. The use of yearly and spatially distributed land cover data that depicts these changes increases the accuracy of hydrological models [6], which are generally used for water resources and flood risk management. Moreover, for rural and ungauged areas, where the influence of humans on the hydrological cycle is higher [7], such analysis is important. However, it is costly and time-consuming to get updated land cover data in highly changing systems. That is the case of Greece, where only 6% of people lived in urbanized areas until 1821 [8] and by 2017 around 80% of the area was urbanized [9].

One way to obtain information is through crowdsourcing, a process in which novel low-cost data can be generated with the support of citizens [10]. The Scent project (<https://scent-project.eu/>, accessed on 1 January 2022) is an example of using crowd observed data [11]. Scent is a European Union (EU) H2020 research project, intending to engage citizens for the collection of data and make them the ‘eyes’ of the decision-makers. Data are also made freely available by different institutions, such as by Copernicus (<https://www.copernicus.eu/en>, accessed on 1 January 2024), the European Union’s Earth Observation Programme. Copernicus produces varied maps at global, European and local level, from which CORINE (coordination of information on the environment) available at <https://land.copernicus.eu/pan-european/corine-land-cover>, accessed on 1 January 2024) is a general land cover map and Urban Atlas is a dedicated sub-product with emphasis on urban areas.

One of the pilot areas considered in the Scent project was the upstream part of the Kifissos catchment, in Greece. In pace with the situation over the country, the urban area increased rapidly in this region, and nowadays, the catchment is about 68% urbanized and continues to further be urbanized [12]. Almost 3.1 million people are living in Athens nowadays [13], pushing towards growth of urban areas and contributing to flooding problems. The catchment’s hydro-meteorological conditions determine low or non-existent river flows for most of the time during the year. However, when short time, intense precipitation events happen, they trigger floods in the catchment [14]. Therefore, the Kifissos catchment is an example of where updated information is important. Through the Scent project, new data in Kifissos were available and can be applied to improve the hydrological models in the catchment. Similarly, the land cover maps produced by Copernicus can also be used and analyzed in their ability to provide updated information for models. Hence, the quality and applicability of those data sources needed to be compared with each other to capture the hydrology in the region.

This research explored the influence of varied land cover data sources in the hydrological modelling of the upstream part of Kifissos catchment by comparing gridded and lumped models. These two representations required different parameterizations, for which land cover sensitivity analysis was carried out.

2. Materials and Methods

2.1. Study Area

The total area of Kifissos catchment is 374.6 km² [15]. The present study focuses on the upper 136 km², upstream of Athens, Greece (Figure 1). Several mountains are located in the area, surrounding the river basin: Parnis (1400 m) in the north, Penteli (1100 m) in the north-east, Hymettos (1000 m) in the east and Aigaleo (400 m) in the west. The basin outlets at the Saronikos Gulf [15], which shows that the catchment contains steep slopes. Kifissos catchment has a Mediterranean climate with an average annual rainfall of 332.2 mm. The main river is 33.7 km, while the river network is sparse [16]. The climatological, geomorphological and anthropogenic factors of the catchment are such that the river becomes dry during most of the time of the year; however, it conveys very large volumes of water within short and intense precipitation events [14].

A study with Landsat imagery, conducted by Chrysoulakis et al. [17], found that the increment in urban area over 20 years (from 1988 to 2007) in the Athens basin was about 30%. This basin used to have six natural river networks drained to a lake; however, rapid urbanization did not take into account those natural water bodies, which were, among others, canalized underground or built over. This had consequences during severe flood events, such as heavy damage in physical properties and lives [18]. In 2019, 68% of the catchment is urbanized, which further increased the flood risk in Athens. Bathrellos et al. [16] studied the flood event of 22 February 2013, during which rainfall reached 100 mm in five hours, the highest in the last 50 years, causing blockades on highways, the metro and train stations, electricity supply shortages and fatalities. On 24 October 2014, due to extreme rainfall, the west side of the catchment was heavily affected.

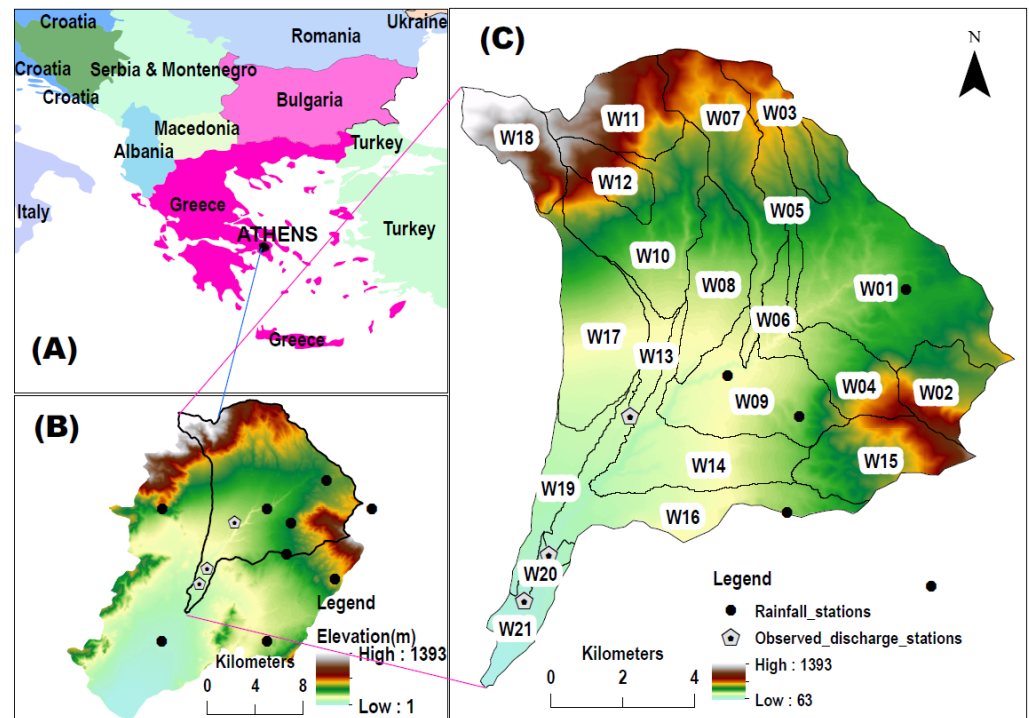


Figure 1. Location map of (A) Greece, (B) Kifissos catchment with delineated study area (bottom left) and (C) study area with 21 sub-basins and observed discharge stations (right).

2.2. Overall Methodology

For the study, the Hydrologic Modeling System (HMS) suite, developed by the Hydrologic Engineering Center (HEC) of the USACE (United States Army Corps of Engineers, Davis, CA, USA), was used. HEC-HMS has already been widely tested, as reported in [19]. Multiple studies show its applicability in different climate regions.

Continuous hydrological models were built using HEC-HMS version 4.9, HEC-DSSVue version 2.0.1 and HEC-SSP version 2.1 software packages. Lumped and gridded model instances were defined based on three different land cover datasets: CORINE (<https://land.copernicus.eu/pan-european/corine-land-cover>, accessed on 1 November 2020), Urban Atlas (<https://land.copernicus.eu/local/urban-atlas>, accessed on 1 November 2020) [20] and Scent.

A lumped model uses parameters that represent spatially averaged characteristics of a hydrological system. They represent only the time variation of a catchment; space is reduced conceptually to a single point. When more detailed spatial information can be included in a model, catchments can be considered divided into cells (grids), where each will act as lumped hydrological models. The contribution of each grid is added together to obtain the response of the whole basin [21]. In HEC-HMS, the DEM differences may lead to different sub-basin delineation, which would produce different level of detail spatially. This could lead to more insights about hydrological processes at the local scale. The number of sub-basins (spatial detail) depends on the data availability and modelling objectives in each study.

In total, based on HEC-HMS software, an instantiation of 12 hydrological models was developed in this study, six lumped and six gridded. Each of these models was set up with 21 sub-basins, to capture the spatial variability of catchment characteristics. The focus here is on variations in land use land cover LULC input data and their impact on the model outputs.

Table 1 presents an overview of the specific differences between these models:

Table 1. HEC-HMS models set-up.

Model Identifier	Lumped or Gridded	Land Cover Data Set
M0LC, M1LC	Lumped	CORINE
M0LE, M1LE	Lumped	Urban Atlas
M0LS, M1LS	Lumped	Scent project
M0GC, M1GC	Gridded	CORINE
M0GE, M1GE	Gridded	Urban Atlas
M0GS, M1GS	Gridded	Scent project

Each developed model has an identifier, M0 or M1, a letter for model structure and parametrization (L for lumped and G for gridded), followed by a letter showing the land cover datasets used in the model (C stands for CORINE, E stands for European Union Urban Atlas and S stands for Scent). Each model instance was built based on two different imperviousness maps, hence identifier 0 and 1. One imperviousness map was based on LULC data and the other was obtained from online sources. Based on data availability, the simulation period was 1 July 2017 to 30 September 2019.

2.3. Available Data

2.3.1. Land Use Land Cover (LULC) Maps

The European Union's Earth Observation Programme (Copernicus), provides the CORINE land cover inventory every four to six years at European level. In this study, the 2018 map was used, with 17 land classes at 100×100 m cell size in the case study area. This study also investigates the value of a sub-product provided by the same institution, the Urban Atlas, which contains details of urban features in vector form with 22 land classes. Lastly, the Scent project involved citizens equipped with a gaming application taking pictures of land cover features, in campaigns organized from September 2018 to June 2019. Together with high resolution satellite imagery, a land cover map was produced using a deep learning algorithm. The generated map has a cell size of 40×40 cm with 4 land classes: bare soil, forest, agricultural land and concrete. By analyzing these three land cover maps (Figure 2), it can be seen that the upstream portion of the basin is more covered with forest, vegetation and agriculture, whereas the downstream is mainly urban with built-up areas. The main difference among these datasets is the distribution and area of land classes, as well as the resolution. The Urban Atlas has a more detailed characterization in classes and CORINE has the largest pixel size, whereas Scent has a smaller pixel size but very few land classes.

Using these three LULC datasets, each with different spatial resolutions, affects the models differently depending on the type of model. In the considered lumped models, the spatial resolution impacts the area proportions of each land cover class within sub-basins, which in turn may influence how certain sub-basin parameters are weighted by land cover class, as detailed in Section 2.5.2. In some cases, the spatial resolution might be irrelevant if both coarse and high-resolution LULC datasets result in similar land cover class proportions. In the gridded models, there are processes calculated within a 500×500 m grid, with most sub-basins covered by 2 to 3 grid cells. As a result, increasing the model resolution allows for greater refinement in hydrological process representation. The impact of spatial resolution on model results is further discussed in the comparison between lumped and gridded models.

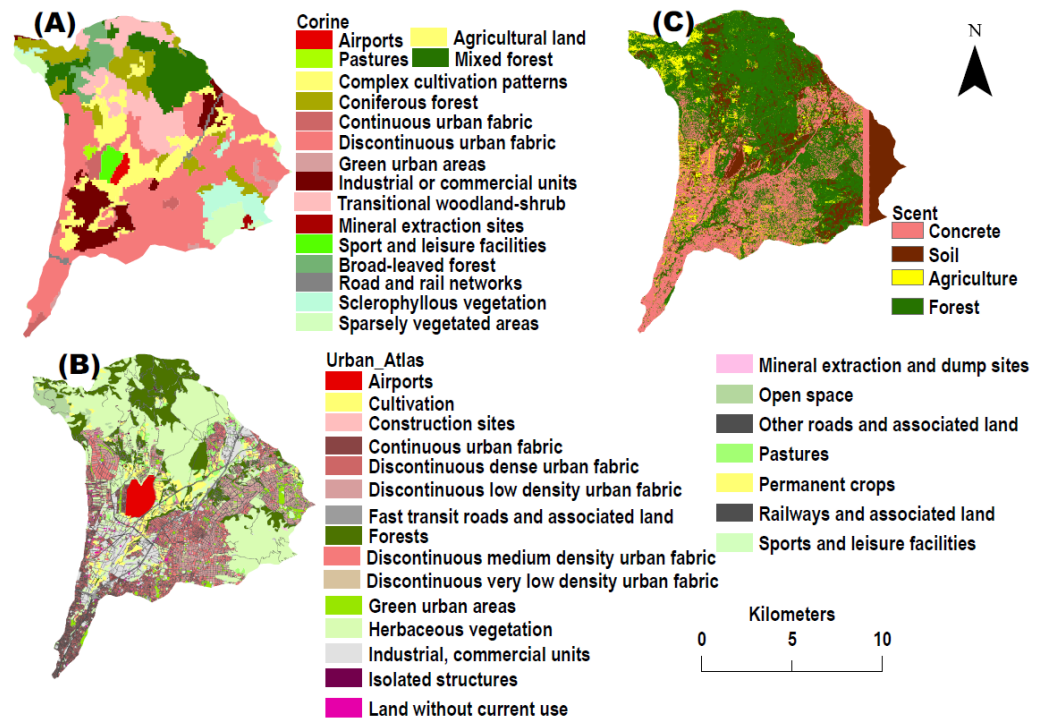


Figure 2. Land use land cover maps for (A) CORINE, (B) Urban Atlas and (C) Scent.

2.3.2. Other Data Types

Two types of imperviousness maps were used to calculate the percentage of the sealed area. The first type was a 100×100 m map, also made available by Copernicus (<https://land.copernicus.eu/pan-european/high-resolution-layers/imperviousness>, accessed on 1 November 2020) [20]. The cell values range from 0% to 96%. The second type of map was generated based on the three different LULC datasets, described in Section 2.5.3.

A hydrologic soil properties map was taken from soil information provided by the European Soil Data Centre (ESDAC) [22]. The European Soil Database (ESDB) was developed in collaboration with the European Soil Bureau Network. Information on the soil texture was used for parameterizing the hydrological models.

The National Observatory of Athens makes available daily precipitation information in Greece, and nine stations were identified near the study area. The north-west side of the basin does not have a rainfall station, and only three stations are inside the basin, fairly well distributed. Averaged monthly data for potential evapotranspiration (ET) were taken from the estimation made by Tegos et al. [23], based on data from a meteorological station located in Athens, around 15 km from the study area. They used varied calculation methods, from which we adopted the Penman–Monteith values since they were the best estimates of potential ET mentioned in their study.

Water depth time series were obtained from three stations by the Scent project (<https://Scent-harm.iccs.gr/>, accessed on 1 November 2020), of which almost 50% of the data are missing from the studied period. The water depth values were then converted to discharges using Manning’s equation and measured river cross-sectional data. The telemetric data were recorded in 15 min intervals, and they were converted to average daily discharge. The locations of the stations (Kokinosmilos, Monastiri and Dekeleia) are presented in Figure 1. The digital elevation map used for the gridded hydrological model has a resolution of 5×5 m. It was provided by the Scent project, which was obtained upon request from Greek authorities.

2.4. Model Setup

The HEC-HMS software has four components in the lumped setup: basin model, meteorological model, control specifications and time series data. The basin model contains

the basin's characteristics, and it is further composed of: canopy, surface, loss, transform and routing. The canopy component includes the parameters of rainfall storage on the canopy, whereas surface deals with the amount of water stored in depressions on the ground. The loss component contains the variables moisture content and the deficit of the conceptual linear groundwater reservoir that simulates the base-flow component. Transform converts the excess precipitation to runoff, and routing represents the conversion of surface runoff to the flow. The meteorological model provides the rainfall, and ET data and control specification specified the starting and ending date and time of the simulation to the model. Similarly, time series data contain the rainfall, ET and discharges. There are additional components for the gridded set-up, terrain data, grid regions and grid data (discretization for gridded models). The grid size of the input files was 500×500 m, which is the minimum grid size available for the gridded transform component. In this case study, the first lumped model was built based on an existing event-based model [24], for which the basin component was modified to better fit continuous simulations and the current datasets.

A simple method applicable to both continuous and gridded basin models is the deficit and constant method, whereby most of the parameters could be calculated based on available data. The method considers the rainfall as the main input in the hydrological process and includes distinct treatments for pervious and impervious areas. When rainfall occurs, the canopy stores some of the precipitation, which either evaporates or infiltrates into the ground. For pervious areas, percolation is dependent upon the soil properties and only occurs if the soil is saturated, and similarly, evapotranspiration only occurs when there is no rainfall and there is moisture in the soil. The soil is represented by a single reservoir and base-flow is added separately. Excess precipitation is generated due to soil saturation. When soil gets saturated and there is still rainfall, then surface depressions retain some of the precipitation. The fluctuation in the linear reservoir is dependent upon the moisture content in the soil from the previous day (or initial condition) and addition due to infiltration or deduction due to evapotranspiration. Once evapotranspiration occurs, water is lost permanently. Over impervious areas, precipitation not intercepted by the canopy becomes excess precipitation. Impervious areas are defined by the percentage of imperviousness.

The model variables are defined by the following equations:

$$C_e = P - C_s \quad (1)$$

$$P_e = P_{imper} + P_{soil} \quad (2)$$

$$P_{imper} = imper \% * C_e \quad (3)$$

$$P_{soil} = (1 - imper\%) * (C_e - I - S_m), \quad (4)$$

when there is no rainfall,

$$MC_t = MC_{t-1} - ET + C_{s-1} \quad (5)$$

and when there is rainfall,

$$MC_t = MC_{t-1} + C_e \quad (6)$$

where

P = precipitation,

Pe = excess precipitation,

imper% = imperviousness percentage,

Ce = excess canopy,

I = infiltration,

MCt = moisture content fluctuation,

MCt-1 = remaining moisture content of previous day or initial condition,

Cs = canopy storage,

Cs-1 = Canopy storage of previous day,

S_s = water available for surface storage,
 S_m = maximum surface storage
 ET = evapotranspiration,
 P_{imper} = excess precipitation due to imperviousness % and
 P_{soil} = excess precipitation due to soil saturation.

Over pervious areas, Equations (5) and (6) for moisture content are used when the reservoir is not full. Once the reservoir is full, percolation into the groundwater starts to occur, which is another variable for permanent loss of water in this model. In the case of a full reservoir, if the excess canopy available for infiltration is higher than the soil percolation, then P_{soil} is activated. Water is available for surface storage, and when maximum capacity is reached, then it starts to produce excess precipitation. Otherwise, the imperviousness alone is responsible for the generation of excess precipitation. In the case of gridded models, the input parameters were given in a gridded form and hydrological processes partially took place over the individual grid. However, the lumped model takes parameters as per sub-basin, but the results of different variables such as excess precipitation, infiltration etc. for both gridded and lumped models were analyzed per sub-basin.

2.5. Input Parameters

2.5.1. Canopy Method

The simple canopy method was adopted where water is stored in leaves when rainfall occurs, and interception continues until the maximum capacity is reached. Due to the geographical position of the catchment, evapotranspiration was set to occur only in seasons with warm temperatures, which are dry periods. The additional rainfall after maximum storage of leaves will fall to the surface. It was calculated individually for all three (Scent, Urban Atlas and CORINE) land cover datasets. The canopy interception values were adopted from Verbeiren et al. [25] and have the storage value per land cover type. For gridded models, raster maps were created by attributing canopy values to each land class cell. For lumped models, the area and canopy type of each land class were determined and the weighted average canopy value for each sub-basin was calculated, as described in the following equation:

$$MC_{S_{sb}} = \frac{\sum_{i=1}^n A_{lci} * MC_{S_{lci}}}{A} \quad (7)$$

where

$MC_{S_{sb}}$ = maximum canopy storage for sub-basin sb,
 A_{lci} = area of land class i,
 $MC_{S_{lci}}$ = maximum canopy storage of land class i,
 A = total area of the sub-basin.

The distribution of maximum canopy storage at the north-west corner of the basin for all LULC datasets seems higher than other parts and lower at the downstream part of the basin.

The crop coefficient is a ratio multiplied with the potential ET to get the actual ET from the soil. Its value was obtained from Nistor et al. [26]. The calculation process and the distribution of data followed a similar pattern to canopy maximum storage.

2.5.2. Surface Method and Loss Method

The surface method was represented by a simple surface process. Initially, surface storage was considered as dry, while the maximum was determined based on its relation to the sub-catchment slope type, according to Bennett [27]. It is noticed that in the downstream and some of the middle part of the catchment, the surface storage is maximum, while in other parts of the basin it is not.

The deficit and constant loss method were used to represent the surface and sub-surface hydrological processes by means of one linear reservoir with three parameters: initial deficit, maximum deficit and imperviousness and percolation rate. The maximum

deficit characterizes the maximum quantity of moisture that the linear reservoir can retain, stated in depth, and is calculated from the curve number (CN), as per in Equation (8).

$$S = (25,400 - 254CN_f) / CN_f \quad (8)$$

where

S = maximum deficit,

CN_f = average curve number for land class.

Curve numbers for different land covers were calculated and estimated from data and from the CN tables of the HEC-HMS technical reference manual [28]. Initial deficit is the initial condition of the moisture depth of the reservoir, and it was taken as 20% of the maximum deficit. Based on the resulting inputs, the CORINE has a higher maximum deficit in the middle part of the basin, whereas for the Urban Atlas, this is noticed in its eastern area. In contrast, for Scent models, the downstream part of the basin presents the highest values. The maximum deficit for CORINE land cover is higher than the other two datasets.

2.5.3. Imperviousness and Constant Rate

All the rainfall occurring in the impervious portion and remaining after canopy storage converts into direct runoff. As mentioned, two types of imperviousness percentage inputs were assessed in this study. The first was generated based on the Copernicus imperviousness map, in which, for lumped models, the average imperviousness for each sub-basin was calculated, and for gridded, upscaling of the cell size from 100 × 100 m to 500 × 500 m was completed. In this case, the same imperviousness inputs were used independently of the land cover datasets. In opposition, USGS imperviousness was calculated individually for each land cover dataset, using the coefficient of imperviousness adopted from Tilley and Slonecker [29]. For the lumped model, the same calculation process of other parameters (weighted average) was followed. For gridded models, raster files were made with the use of imperviousness coefficients. The upscaling of land cover for 500 × 500 m was performed by taking the average of all the pixels of land class located inside the grid and then attributing the obtained value to imperviousness. All the maps have a similar nature whereby the downstream portion of the basin is more impervious than the upstream part.

The constant rate indicates the percolation rate in mm/hr for the model, and they were taken from the soil physical properties information from the study conducted by Elnesr [30]. For this analysis, textural information about soil was needed, and that information was taken from ESDB map.

2.5.4. Transform Method

The Clark unit hydrograph and Modclark methods were chosen to represent overland flow processes for lumped and gridded models, respectively. The parameter time of concentration was calculated by taking the values of lag time, taken from the existing event-based model [24], divided by 0.6 [31]. Similarly, storage coefficients which account for storage effects were calculated by dividing the average observed flow (of three observed stations) at inflection points on the falling limbs of several flow peaks by the time derivative of the flow. The time derivative was obtained by the difference in flow at the point of inflection and the flow during the next day divided by time (1-day interval).

2.6. Model Calibration and Validation

As the objective of this study is to investigate the influence of land cover on hydrological processes, parameters defined based on data were not calibrated. The lumped and gridded CORINE-based models (M0LC and M0GC) were calibrated and validated. Calibrated parameters were used in further model instances. Calibration of the following parameters was performed:

- Transformation method: time of concentration and storage coefficient
- Base-flow method: initial discharge, recession constant and ratio to peak

The total simulation time was about 27 months (1 July 2017 to 28 September 2019). Since there was a lot of absence of data, the longest time of available data was about six months (28 September 2017 to 31 March 2018), and hence, it was chosen for calibration. Similarly, the period of 14 September 2018 to 12 January 2019 was chosen for validation.

Calibration was performed manually, by comparing simulated and observed flow hydrographs at the three water depth stations. Three discharge stations, shown in Figure 1, were used for calibration: Kokinosmilos (J09), Monastiri (J12) and Dekeleia (J08). The calibration was guided by the physical characteristics of the case study and of each sub-basin: steepness, level of urbanization or forestation and depth to the groundwater table (GWT). The final calibrated values for lumped and gridded models are shown in Table 2, and the results obtained after calibration and validation are shown in Figure 3. For both approaches, lumped and gridded models, the obtained value for the ratio to peak for all sub-basins is 0.5 and the recession constant is 1. The base flow for lumped and gridded models matched, whereas the peaks of observed flow are higher for both calibrated and validated models. Similarly, the starting time of the peak for all models is the same. From the calibration of lumped and gridded models, it was found that almost all the parameters were the same except the initial discharges. The initial discharges for gridded sub-basins were higher.

Table 2. Final calibrated input values for lumped and gridded.

HEC-HMS Sub-Basin	Steepness	Urban	Rural	GWT	Initial Discharge Lumped (m ³ /s)	Initial Discharge Gridded (m ³ /s)	Time of Concentration (h) for Both	Storage Coefficient (h) for Both
W01	M	M	M	H	0.02	0.3	8.7	5.9
W02	H	M	M	L	0.01	0.2	14.8	5.9
W03	L	L	H	L	0.01	0.2	15.5	5.9
W04	H	L	H	H	0.04	0.2	24.3	5.9
W05	H	L	H	L	0.02	0.3	17.8	5.9
W06	M	L	H	H	0.02	0.2	10.5	5.9
W07	H	L	H	L	0.03	0.2	7.1	5.9
W08	M	L	H	H	0.05	0.2	2.4	5.9
W09	L	H	L	H	0.05	0.2	4.4	5.9
W10	H	L	H	H	0.03	0.01	1.9	13.4
W11	H	L	H	L	0.01	0.03	13.2	13.4
W12	H	L	H	L	0.02	0.03	13.8	13.4
W13	H	H	L	H	0.03	0.02	12.2	13.4
W14	L	H	L	H	0.02	0.22	2.2	5.9
W15	H	L	H	L	0.04	0.22	8.7	5.9
W16	L	H	L	H	0.05	0.22	31.1	5.9
W17	L	H	L	H	0.1	0.05	1.9	10.4
W18	H	L	H	L	0.1	0.05	13.2	10.4
W19	M	M	M	H	0.1	0.05	10.8	10.4
W20	H	H	L	H	0.04	0.04	5.9	10.4
W21	L	H	L	H	0.1	0.1	1.7	10.4

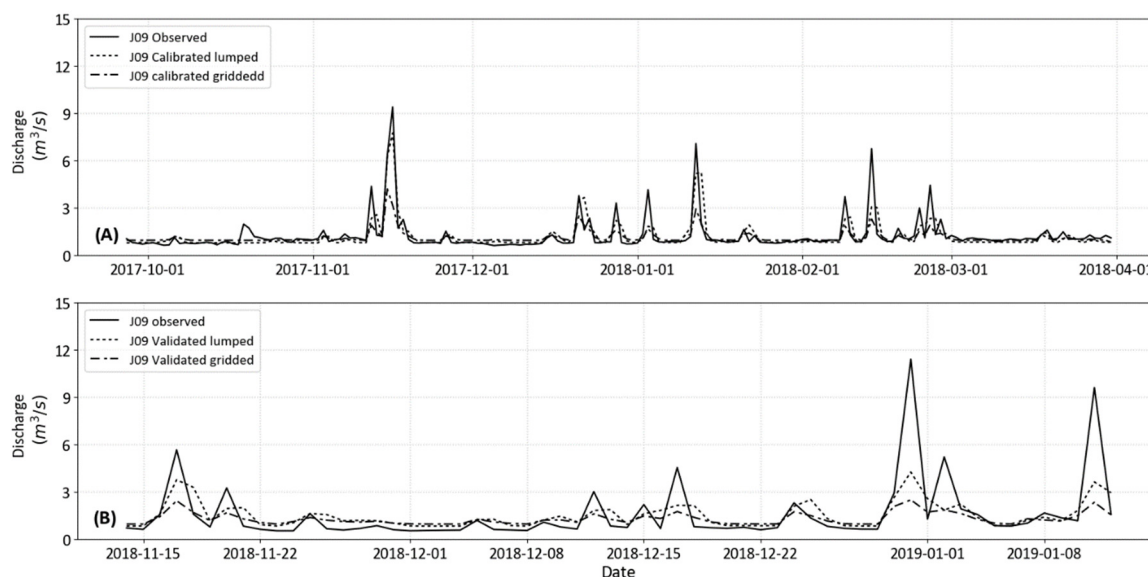


Figure 3. (A) Calibration of basic lumped and gridded models and (B) validation of lumped and gridded models.

3. Results and Discussion

3.1. Land Cover Influence on Hydrology

3.1.1. Hydrological Processes

The representation of hydrological processes can be completed using several variables such as excess precipitation, evapotranspiration (ET) and moisture fluctuation in the reservoir. Although there are 12 models and each has 21 sub-basins, for this analysis, sub-basins W08, W03 and W20 of M0LC: CALC (lumped model with CORINE land cover and calculated imperviousness) are chosen because of their land class distribution. W08 is a mixed sub-basin, having urban, forest and agricultural areas, whereas W03 is 99% forested and W20 is 100% urban area. It is important to note that urban areas do not have a one to one relation with imperviousness, because they can contain pervious land associated with urban areas. Therefore, W03, W08 and W20 have 12.1%, 27.2% and 72.2% imperviousness, respectively. The analysis of hydrological processes was completed for the whole simulation period; however, results for a representative time interval (November 2018–January 2019) and for sub-basin W08 are presented.

The graph in Figure 4 shows all the main variables taking part in the hydrological processes in the case study area. The canopy storage fills up and empties quickly before and after a rainfall event, respectively. It takes a while to generate excess precipitation due to soil saturation (P_{soil}) because the soil is full only after a few rainfall events and when the highest event occurs above 30 mm. Therefore, for most of the cases, excess precipitation (P_e) comes from the imperviousness percentage of the sub-basin. As mentioned, the water remaining after canopy storage which falls onto the impervious surface converts into P_e . Because Greece is located in a temperate region, when rainfall stops, ET gets activated, and the moisture in the soil starts to decrease until the next rainfall event occurs, which can be seen for 10 days, before 4th December, although the decrease in moisture is small in this period. The fluctuation of the linear reservoir continues until the available moisture reaches its maximum limit. Once it is full and rainfall still continues, then soil percolation starts, which is about 70–80% of rainfall intensity, which is the second half of Figure 4C.

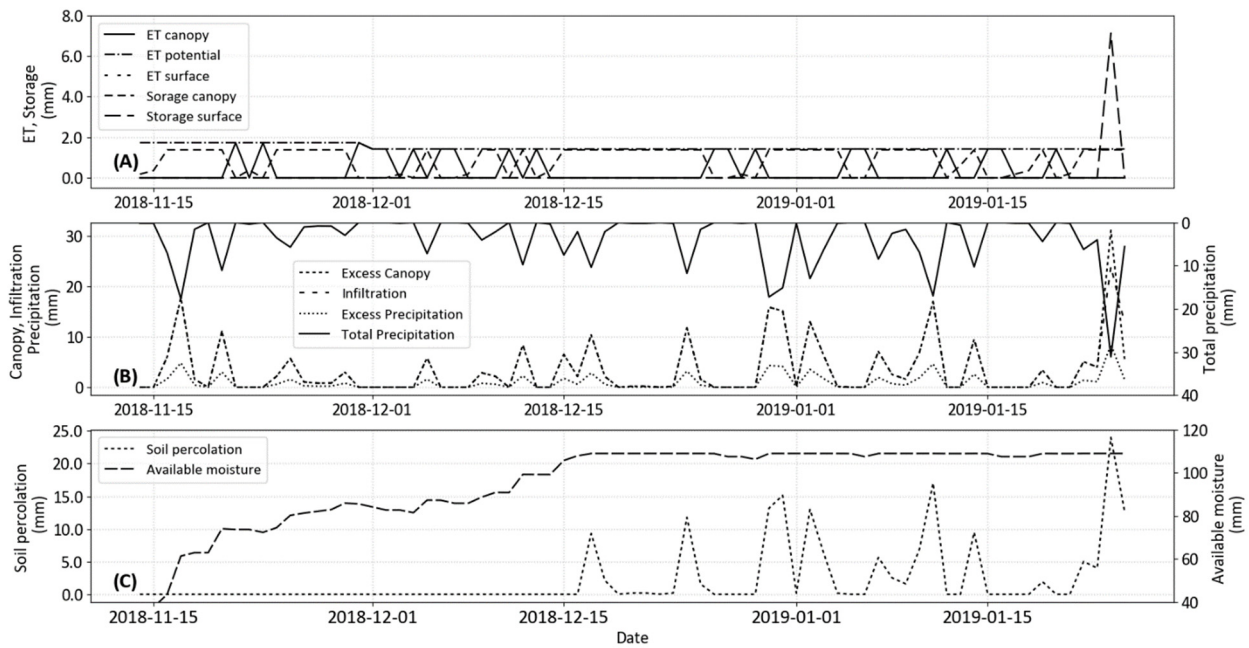


Figure 4. Results of all variables for W08: (A) ET canopy, canopy storage, ET potential, ET surface and surface storage; (B) total precipitation, excess canopy, infiltration and excess precipitation; and (C) soil percolation and available moisture.

In this catchment, after the reservoir is full, almost all of the infiltrated water is percolated first, which can be seen in the graph after the 31st of December until the 23rd of January. However, on 24 January, the excess canopy is higher than the infiltration and this difference becomes the surface storage (Figure 4A). Further, since the maximum surface storage of 12 mm is not satisfied by this amount of surface storage (7 mm), P_e due to soil saturation does not occur in this instance.

For the whole simulation period, 73% of precipitation was lost either due to evapotranspiration (46%) or due to soil percolation (27%), and there is excess precipitation due to imperviousness (P_{imper}) only. Soil saturation also creates some excess precipitation, but it is zero for this sub-basin.

3.1.2. Sub-Basins Comparison

Sub-basins W03, W08 and W20 were compared, as shown in Figure 5. Since W03 has more forest than the other sub-basins, it has the highest canopy storage, and W20 has the lowest, because of its extensive urban area. The behavior of the canopy storage for W20 around 14th of December is different, because there was a very small amount of rainfall in the sub-catchment at that time (0.04 mm), while in the other sub-basins, there was no rainfall. Therefore, the precipitation pattern in the whole basin slightly influences the canopy storage; however, the main factor in this process is the maximum canopy storage according to the land cover. The surface storage for most models and sub-basins is zero for most of the time, but when there is rainfall for several days and the intensity is around 30 mm for at least one day, only then it can be seen (Figure 4A).

In Figure 5C, the excess canopy exactly matches the infiltration for this period; however, they are different for some of the time of the whole simulation, and an example is has already been seen on 24 January 2018. The amount of excess canopy or infiltration for W03 is higher because this sub-basin receives a higher amount of rainfall than W20 and W08.

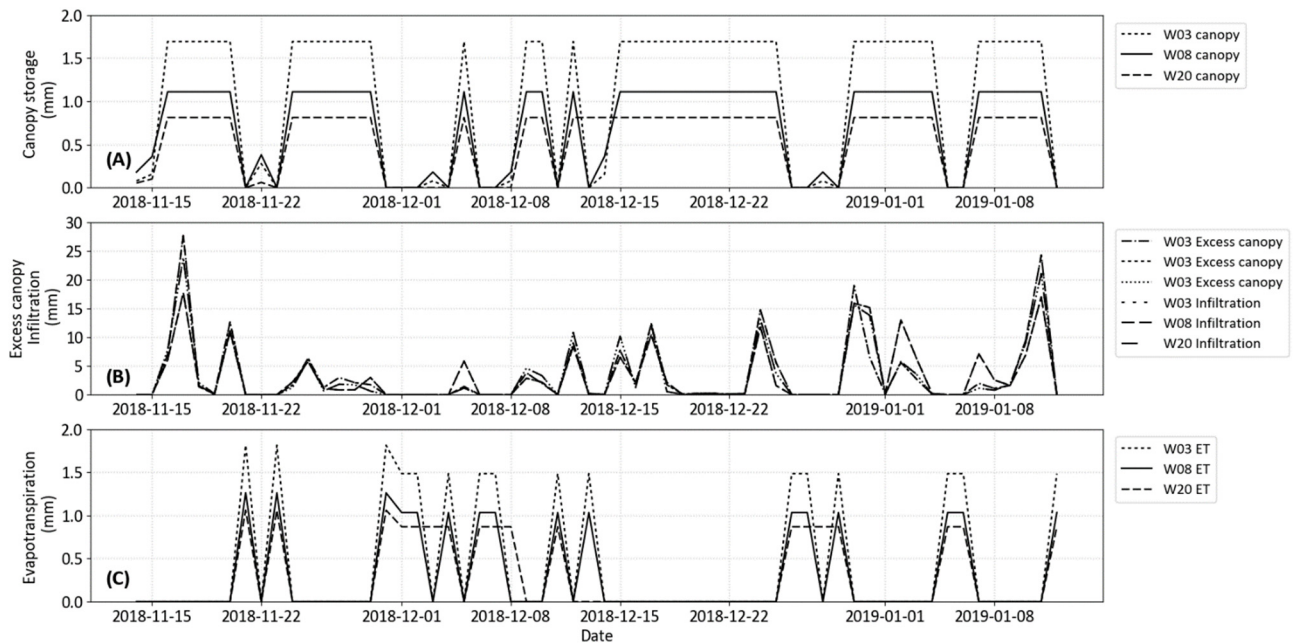


Figure 5. (A) Canopy storage, (B) excess canopy and infiltration and (C) evapotranspiration for W03, W08 and W20 of M0LC:CALC.

Similarly to the canopy storage, the large area of forest coverage of W03 implies a larger potential ET than for the other areas. It converts 65% of its total rainfall to ET, whereas W20 transforms 15%. Thus, the actual ET can reach 2.5 times more for W03 than W20, mainly when the rainfall amount is higher than their respective canopy storage amounts. Therefore, land cover plays an important role in converting rainfall into ET, and a nearly 100% forest area can convert more than 4 times than a nearly 100% urban area.

The maximum storage values for the three sub-basins, which are based on different land classes, are 89.2 mm for W20, 91.1 mm for W03 and 108.9 mm for W08. The sub-basin W08 has the biggest reservoir among the three sub-basins, and it takes a longer time to get saturation. W03 has the medium reservoir so it takes a shorter time to saturate than Urban Atlas. However, W20 has the smallest reservoir and takes the shortest time to fill, and as shown in Figure 6B, when the reservoir is full, it immediately starts to percolate water, which can be seen in the first part of the graph. By comparing W03 and W08, the influence of the size of the reservoir for soil percolation is visible because W03 takes about one week to fill the reservoir and W08 takes more than one month to fill it. Therefore, the urbanized land cover sub-basin fills up quicker than the mixed and forested ones. The urban sub-basin (W20) has a higher amount of excess precipitation (P_e) than the others. The difference in the peak of the total precipitation and P_e is 1.4 times, and about 70% of the total precipitation is converted into P_e . On 24 January, since the soil gets saturated quickly and there is a difference in excess canopy and infiltration (11.3 mm) and greater than maximum storage (9.9 mm), there is generation of P_{soil} . However, the amount of P_{soil} is negligible compared to that of P_{imer} . In contrast, forested sub-basin W03 has the lowest amount of P_e , the difference in the peak is high, which is 5 times, and only about 11% of the total precipitation is transformed into P_e . The mixed sub-basin W08 has a medium amount of transformation to P_e and it is about 25% of the T_e .

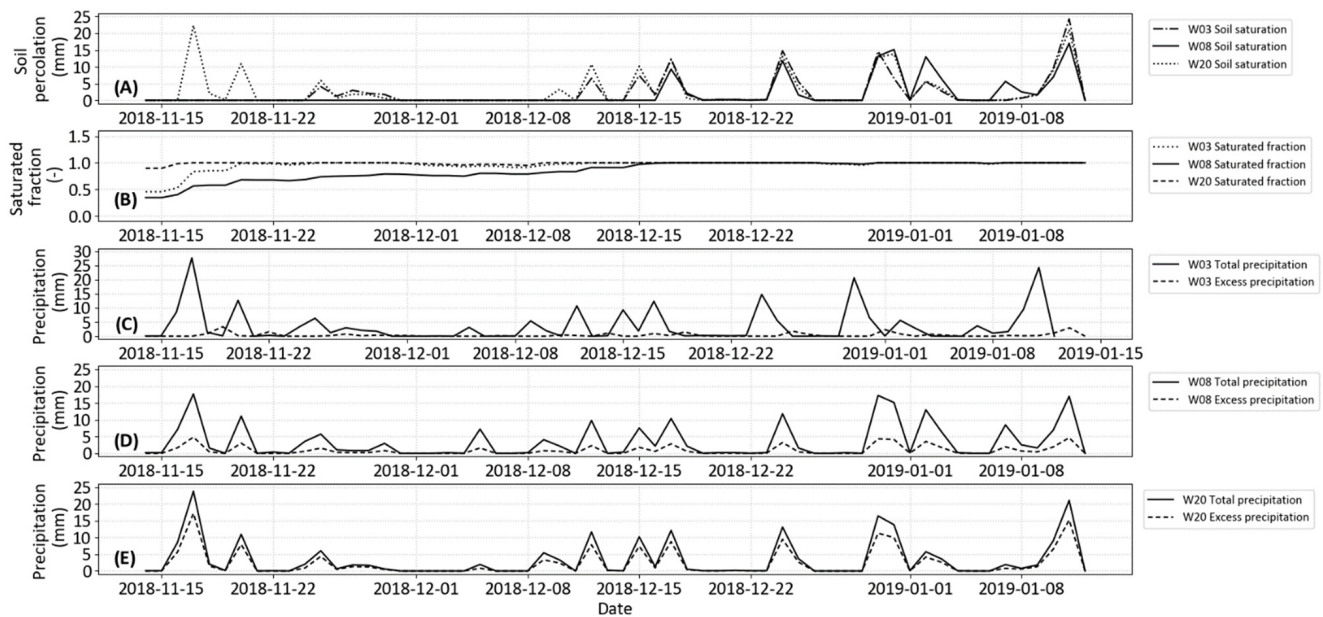


Figure 6. (A) Soil percolation, (B) saturated fraction for W08, W03 and W20 and total and excess precipitation for (C) W08, (D) W03 and (E) W20.

3.1.3. Further Analysis of Excess Precipitation

The P_e along with the imperviousness percentage and soil saturation for all 21 sub-basins are analyzed. The spatial variation of these values and the breakdown into P_{imper} and P_{soil} are shown in Figure 7. Over the whole catchment (Figure 7A), the rainfall occurring for each sub-basin varies between 1266 mm (middle parts) and 1995 mm (upper parts) and has an average value of 1600 mm (downstream parts). P_{soil} is higher (90 mm) in the north-east part of the catchment (Figure 7D), and similar behavior is observed in sub-basin W18. The sub-basins W18 and W15 have a small reservoir, of about 55 mm and 75 mm, whereas W02 and W04 have a large reservoir, but they store more total precipitation than other parts of the basin. P_{imper} has a similar spatial distribution to P_e , with reduced but significant magnitude, while P_{soil} accumulates very small and, for most of the basin, negligible amounts. In contrast, the north-west portion of the catchment has the lowest amount of excess precipitation compared to other parts because it has a highly forested area, which causes more loss due to ET. The areas furthest upstream and downstream have the maximum P_e because the upmost portion receives more rainfall and the downstream part has a higher imperviousness coverage.

In conclusion, regardless of how impervious a sub-basin is, P_{soil} does not pass 20% for all sub-basins and does not pass 5% for 75% of the sub-basins. The main reason is that the soil has great retention ability and percolation capability. Thus, imperviousness and consequently land cover are highly predominant factors in defining excess precipitation.

3.2. Sensitivity to Land Cover Datasets

A sensitivity analysis for three LULC datasets was conducted for the sub-basin W08 of M0LC:CALC, M0LE:CALC and M0LS:CALC models. By varying the land cover dataset, the main parameters that changed are the maximum deficit and imperviousness percentage. Therefore, mainly the variables affected by them were analyzed, which are P_e , potential ET and change in the linear reservoir. The ET for Scent is higher than for the other two datasets shown in Figure 8A. This is because it has the biggest forest area coverage (72%). However, Urban Atlas also has similar ET because of having a significant amount of vegetation (54%) and small coverage of agriculture (11%) and forest (13%), all of which also contribute to ET. In the case of CORINE, there is a less combined contribution for ET than other datasets from all land classes, so it has the lowest amount. Similarly, Scent linear reservoir is filled up first and fluctuation occurs more rapidly and frequently, which can be seen in

Figure 8C, as it has the smallest reservoir (42.9 mm) and the highest ET among all the LULC datasets. In contrast, the CORINE land cover has the biggest linear reservoir (108.92 mm) and the lowest amount of ET, thus taking a longer time to fill up than the other LULC datasets. Whereas Urban Atlas has a reservoir size of 60.41 mm and ET similar to Scent, variations in the reservoir level are intermediate between these two cases. The Pe for Urban Atlas is slightly higher than CORINE, while for Scent, the Pe is low, which correlates with the imperviousness calculated for their associated models. Despite that, the amount of excess precipitation is only up to a third of the total precipitation, with most being lost to percolation. In this whole analysis, P_{soil} is not found in the quantifications.

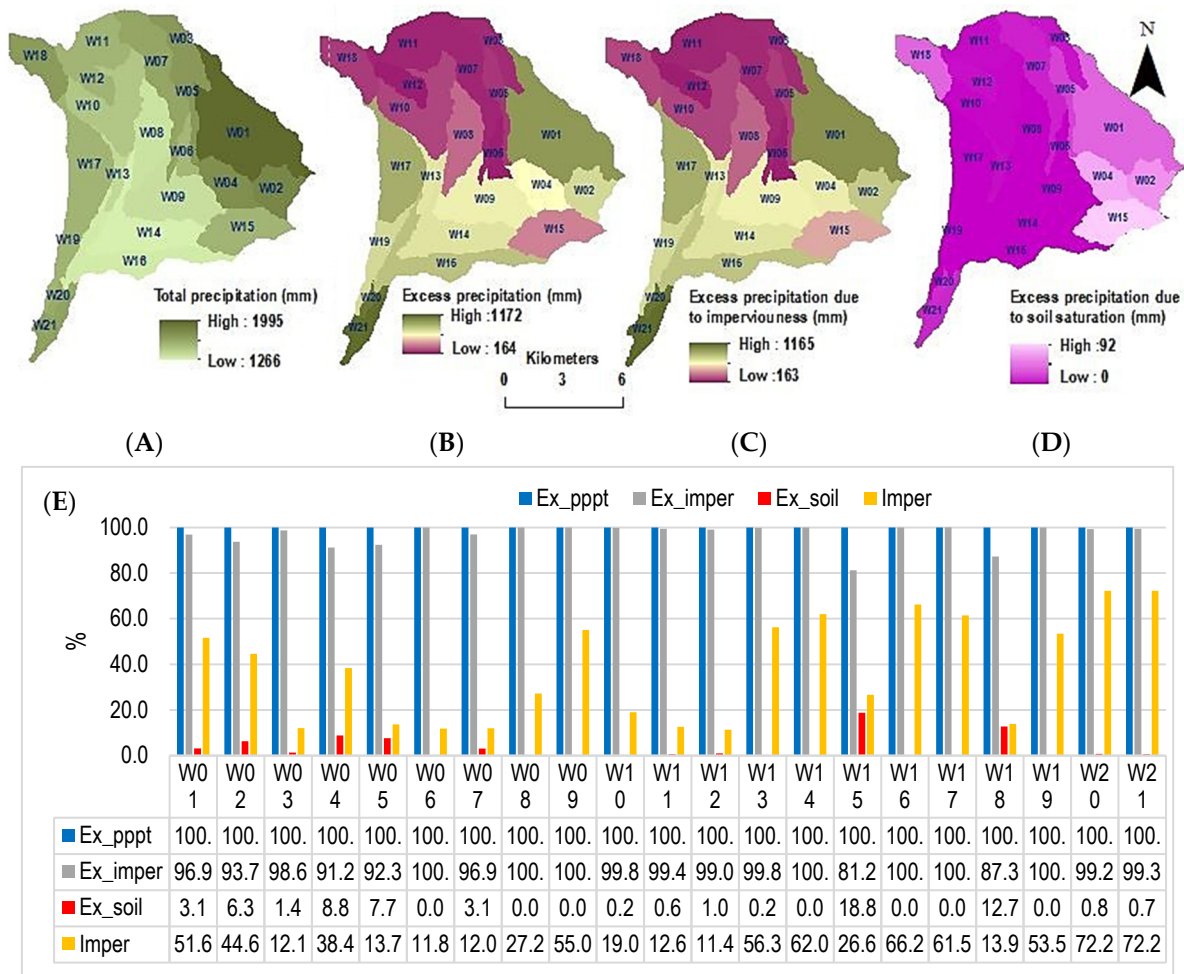


Figure 7. Precipitation distribution pattern for (A) total, (B) excess, (C) excess precipitation due to imperviousness, (D) excess precipitation due to soil saturation and (E) precipitation and imperviousness for all 21 sub-basins in percentage.

3.3. Lumped vs. Gridded Models

The main input parameters that changed with the gridded models are maximum deficit and imperviousness percentage. Other parameters given in gridded form are canopy storage, crop coefficient, surface storage, initial deficit and percolation rate, which do not play a significant role in overland land flow processes.

The ET of the lumped models for all LULC datasets is 1.8 times higher than the gridded models, depicted in Figure 9A–C, because the crop coefficient for all the grid cells are different, whereas only one value is given for lumped models. Similarly, the reservoir of the gridded models saturated faster than the lumped models, mainly when using Scent and Urban Atlas land cover (Figure 9D–F). This is because the infiltrated water is responsible for only one cell to fill up for gridded models, whereas for the lumped

models, the equivalent of the entire area should be filled up to be saturated. The amount of excess precipitation generated in the lumped and gridded models for CORINE and Scent are almost equal; however, for Urban Atlas, the lumped model produces about 60% of the amount of the gridded model, as shown in Figure 10A–C. The main reason behind this is due to the difference in the imperviousness percentage in W08 for lumped and gridded models. Figure 10E–G presents the spatial distribution in the gridded model, where the basin’s imperviousness for CORINE, Urban Atlas and Scent are 28%, 24.5% and 16.8%, respectively. In the lumped model, they are 27.23%, 28.56% and 15.5%, respectively. Therefore, the gridded Urban Atlas model has around 4% higher imperviousness than the lumped one.

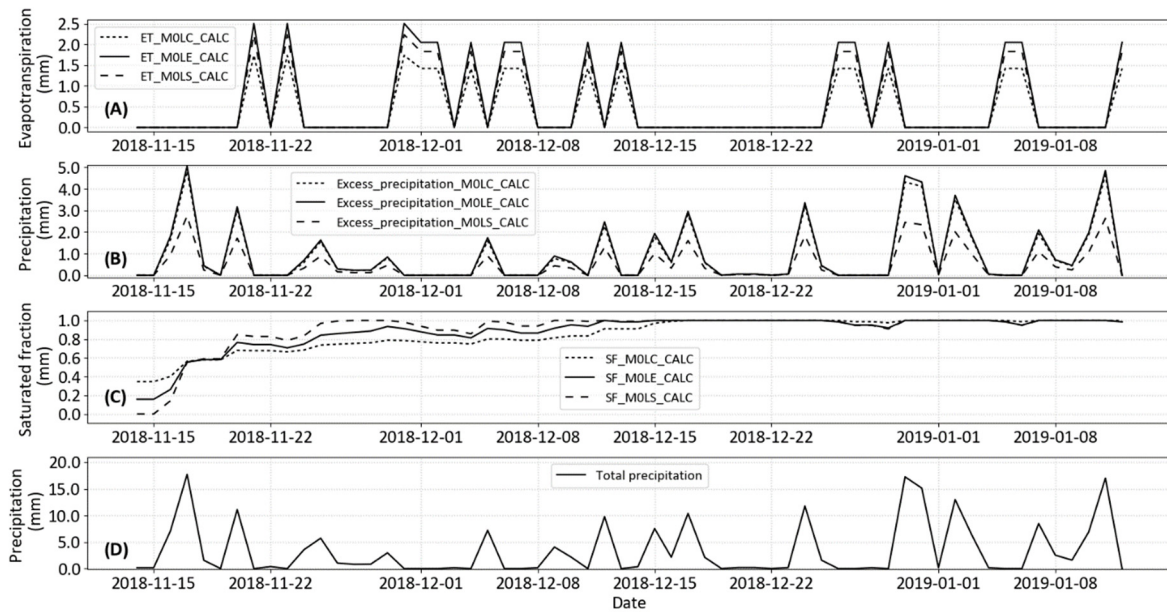


Figure 8. Variables for CORINE, Urban Atlas and Scent models for W08 M0LC:CALC, M0LE:CALC and M0LS:CALC: (A) evapotranspiration, (B) excess precipitation, (C) saturated fraction and (D) total precipitation.

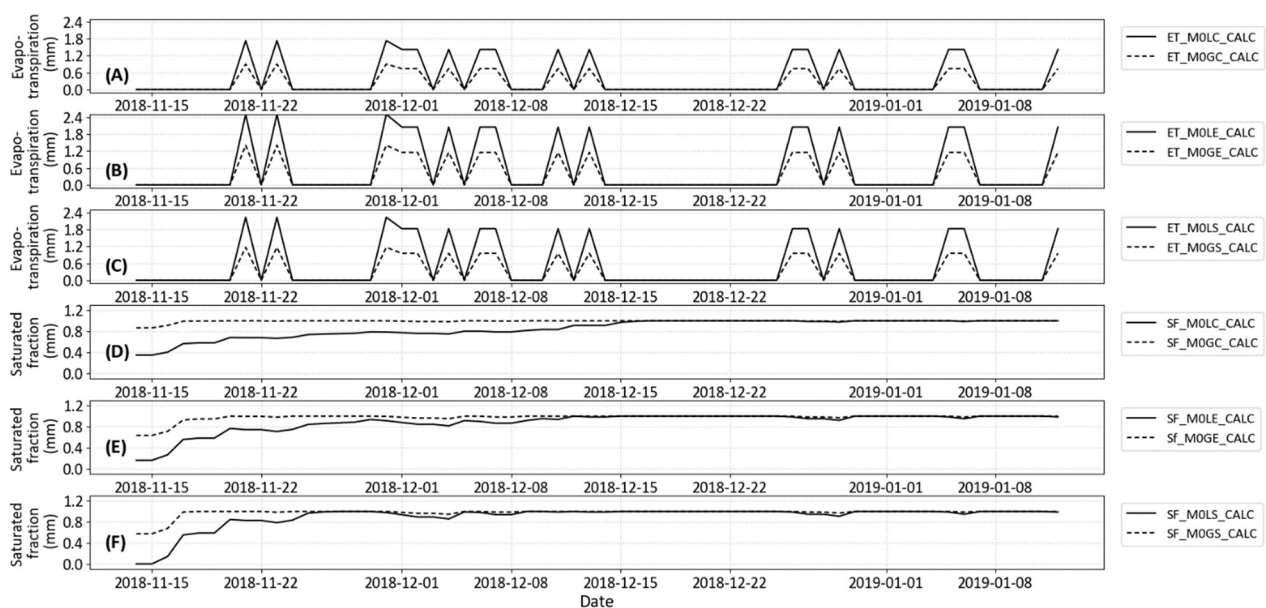


Figure 9. Lumped vs gridded evapotranspiration for sub-catchment W08 for (A) CORINE, (B) Urban Atlas and (C) Scent and saturated fraction for (D) CORINE, (E) Urban Atlas and (F) Scent.

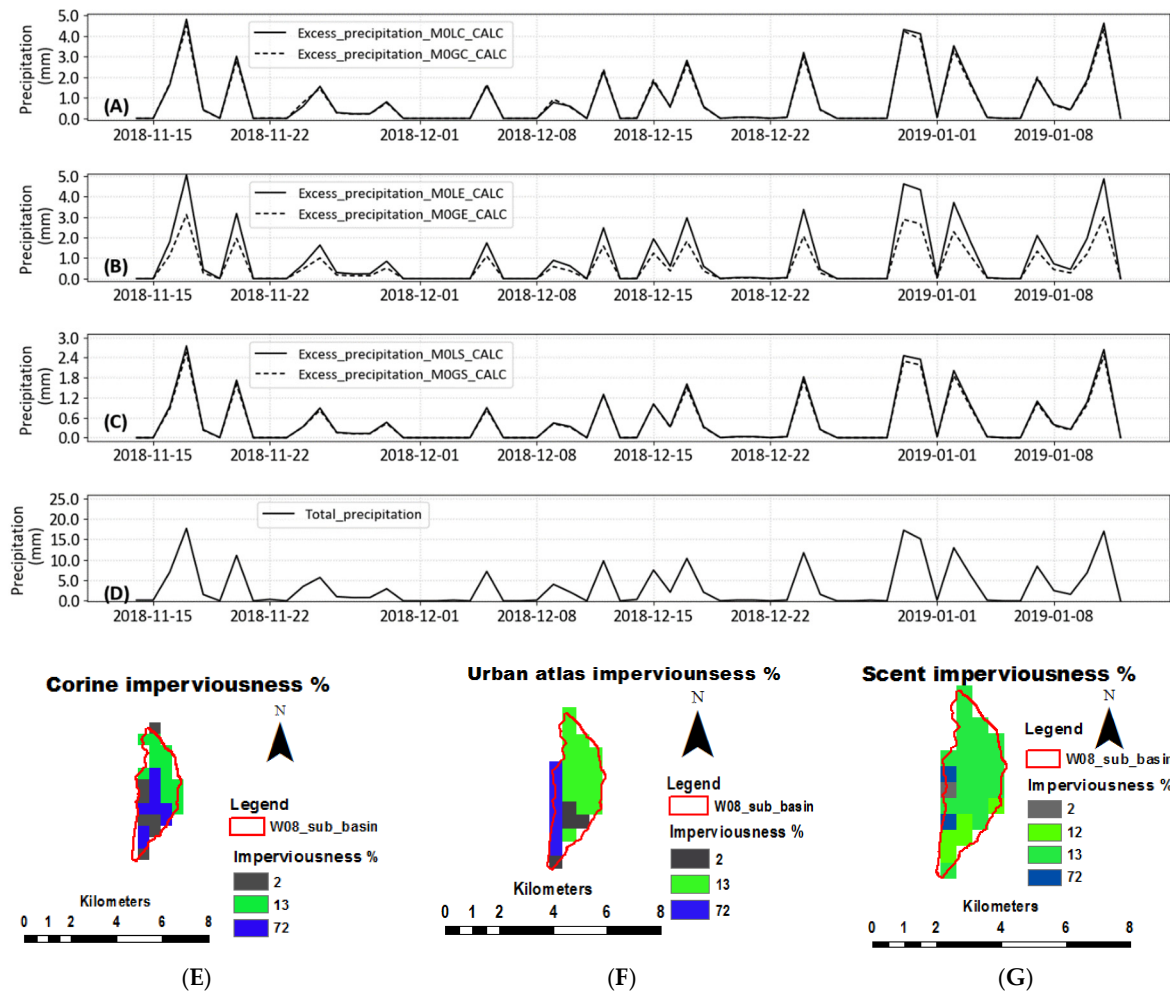


Figure 10. Excess precipitation for W08 for (A) CORINE, (B) Urban Atlas and (C) Scent and (D) total precipitation and imperviousness percentage for W08 for (E) CORINE, (F) Urban Atlas and (G) Scent.

For the cases of the gridded and lumped models, the imperviousness also played an important role in the generation of excess precipitation, which can be precisely observed in the case of Urban Atlas.

3.4. Runoff Flow Analysis

The surface runoffs generated due to excess precipitation for W08, W03 and W20, displayed in Figure 11, are quite similar because of having an identical rainfall pattern. The amount of runoff is analyzed in terms of the areas of the sub-basins, which are 6.9, 3.7, and 0.95 km² for W08, W03 and W20, respectively. As the biggest basin, W08 generates more runoff than the other sub-basins despite not being the most impervious. Regardless, all sub-basins contribute very small amounts of surface runoff to the outlet. Before analyzing flow, it is important to highlight that flows at junctions are influenced by a lot of parameters of routing and transformation, which were calibrated for the CORINE LULC model only. Overall, as depicted in Figure 12, the starting of the peaks matches for lumped and gridded models for J09, and there is one day shift in the observed flow in J08. For J09, a trend is visible in the data; in Figure 12, simulated peaks from the lumped models just after 16 November 2018 are higher than the observed ones, while lumped simulated peaks at a later moment (i.e., after 28 December 2018) are of the same magnitude as the observed peaks. The same decreasing trend is visible in the gridded simulation results. For the case of J08, observed flows are significantly lower than all simulated flows, for both lumped and gridded models.

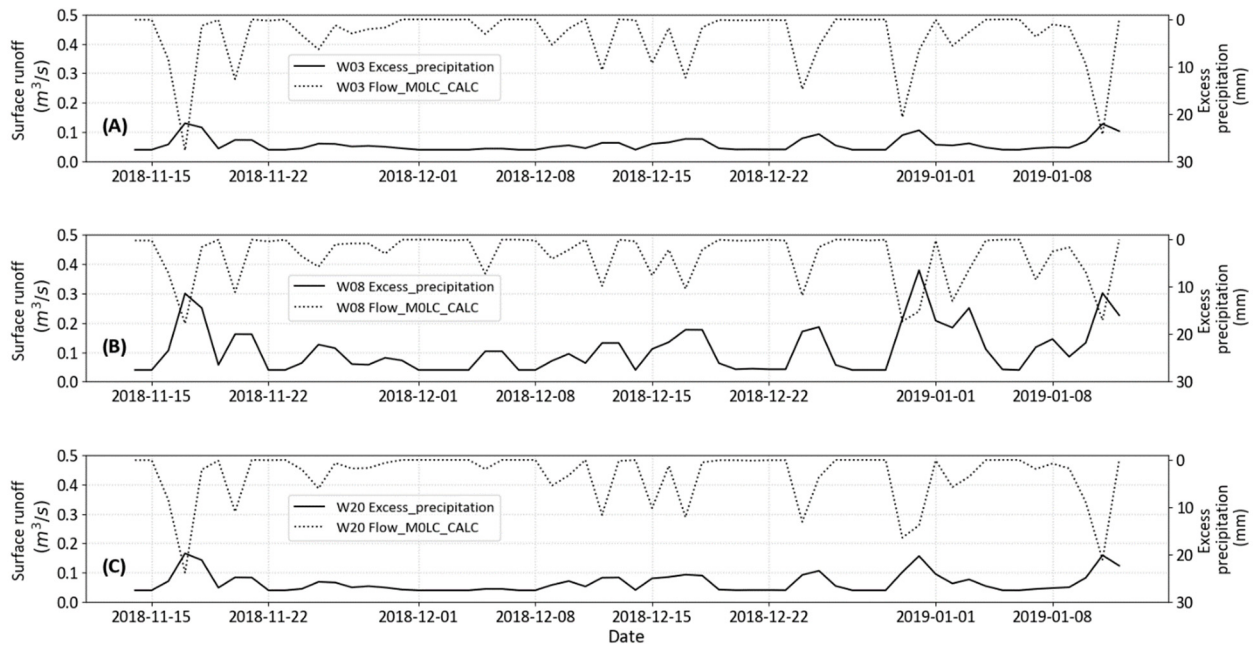


Figure 11. Precipitation vs surface runoff for M0LC_CALC: (A) W08, (B) W03 and (C) W20.

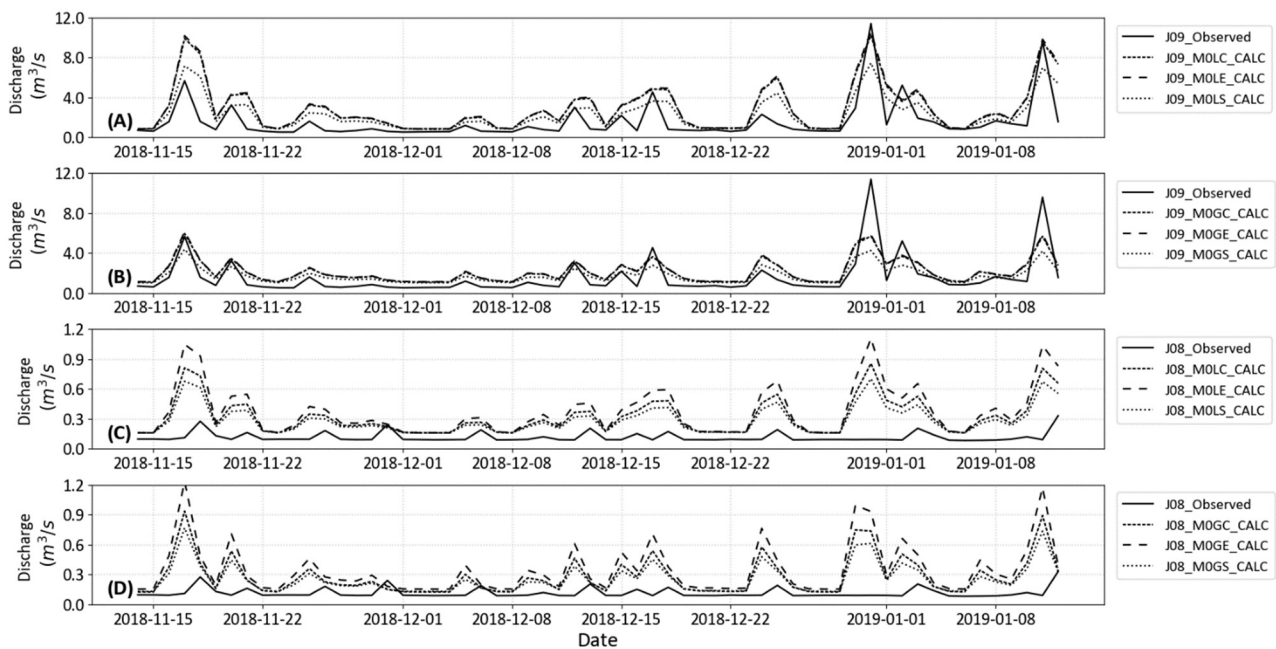


Figure 12. Lumped and gridded models flow for J09, (A) lumped vs observed and (B) gridded vs observed, and J08, (C) lumped vs observed and (D) gridded vs observed.

The CORINE and Urban Atlas models have similar flows in J09, and the reason can be attributed to their similarity in imperviousness. However, for the case of Scent, it has only four divisions of land class, and whole datasets have more pervious land classes than others. Therefore, Scent has the lowest flow compared to the other datasets. In contrast, the discharge of only four sub-basins is collected at J08, leading to what seem to be more marked differences; however, the discharge values are very low, and uncertainties could also be the cause of these differences. Despite differences in magnitude, the pattern for all three datasets is similar.

4. Conclusions

The analysis of the hydrology of three different sub-basins having different characteristics gave insights into three main questions, which are detailed below. This section then gives an assessment of the limitations and future perspectives.

How land cover affects the structure and parameterization of Kifissos hydrological models?

The models describe hydrological processes that allow for canopy storage, infiltration, sub-surface storage with soil percolation (represented by a linear reservoir), evapotranspiration and excess precipitation. Canopy storage is different for each type of land cover; however, its influence in the models is small and does not affect the excess precipitation. All precipitation that is not stored in the canopy infiltrates into the ground through pervious areas. The infiltrated rainfall, actual ET and the maximum deficit (i.e., the reservoir size) control the moisture content of the linear reservoir. All these variables and parameters are different according to each land class. In a forested sub-basin (70% forest), ET resulted in 65% of the total precipitation, which is 15% more than the results for a sub-basin with mixed land cover and 4 times more than those of an urban sub-basin. This difference in ET and the difference in the size of the reservoir causes the saturation of the soil and then percolation at different times. The sub-basin with mixed land cover takes a longer time for the soil to saturate than the urban and forested ones because it has the biggest linear reservoir and considerable ET. The small reservoir at the urban sub-basin filled up quickly and kept full for longer, due to lower ET. When there is soil saturation, percolation processes are dominant and account for most of the reservoir losses during wet periods. This process is not influenced by land cover. Further, when the excess canopy was greater than the infiltration because the maximum percolation rate had been reached, surface storage occurred, which accounted for small volumes. The precipitation from pervious areas, i.e., from soil saturation, is very small regardless of land cover.

Excess canopy over impervious ground does not allow the water to penetrate the soil and is directly converted into excess precipitation. Therefore, the urban sub-basin, which is highly impervious, generates 69.9% excess precipitation, while the sub-basin which is less impervious (the forested one) produces 11.3% excess precipitation.

For all basins in all models, the generation of excess precipitation is highly dependent on the excess precipitation caused by imperviousness (and, consequently, proportional to imperviousness percentages themselves). The minor differences are caused by excess precipitation from soil saturation, which comes from the perviousness percentage of the ground surface.

How sensitive were the hydrological models to changes in land cover from different data sources?

The parameters that changed with the LULC datasets were canopy storage, imperviousness, maximum deficit, potential evapotranspiration and crop coefficient. Different parameters influenced infiltration, fluctuation in the linear reservoir and excess precipitation. From the results, the maximum deficit and imperviousness percentage play important roles and are lower in the Scent data. Reservoirs filled up earlier and generated more excess precipitation from soil saturation than for CORINE, which has a larger reservoir and higher imperviousness percent. Urban Atlas and CORINE have a similar nature in terms of excess precipitation because their imperviousness percentages are similar; however, the linear reservoir fills up first in Urban Atlas because of its smaller size than CORINE. Although the land cover data sets influenced hydrological processes in pervious areas by influencing the size of the reservoir, similarly to the discussion in the previous research question, there is the contribution of excess precipitation due to the saturated soil condition, but they are insignificant. Therefore, in this analysis, the main dominant process for the generation of excess precipitation is also imperviousness.

Hence, it is found that the main parameter playing a role for both sensitivity to land cover and parameterization was imperviousness.

What are the key differences between gridded and lumped model representation, under three land use land cover datasets?

The main difference between gridded and lumped representation comes from the semi-distributed and distributed patterns of the sub-basins. In lumped models, a weighted average of all the land classes within one sub-basin was taken, whereas a separate value was given for the case of gridded models for the calculation of some parameters. The ET of CORINE, Urban Atlas and Scent lumped models are higher than from gridded models for all the cases, and the linear reservoirs of gridded models are filled up earlier than the lumped models.

Similarly, due to the rasterization and making cell sizes of 500×500 m, the actual representation of the land class deviates in gridded models, which resulted in the different amounts of imperviousness and, consequently, of excess precipitation, especially in the case of Urban Atlas. The Urban Atlas gridded model is less impervious and has less excess precipitation than in the lumped one. Furthermore, the excess precipitation due to soil saturation for both models is insignificant compared to the imperviousness percentage.

In conclusion, although the parametrization as a lumped and gridded model also affected the representation of hydrological processes in pervious areas, it was not relevant in terms of excess precipitation.

Future research work and perspectives

Present work shows that if the model was to be used for analyzing hydrological changes under climate change scenarios, the changes would be introduced in the forcings of the model, such as precipitation and temperature (potential evapotranspiration). Considering the focus of our study, which is LULC data, the most sensitive input in all models is imperviousness. Different case scenarios of imperviousness could be generated by changing the area covered by forest or a paved surface. The outcome excess precipitation could be analyzed and compared using different case scenarios.

HEC-HMS itself is a physically based model; therefore, artificial intelligence methods cannot be used in the model itself, but HEC-HMS can add input to a hydrological artificial neural network (ANN) model, for example, to provide training data or in a hybrid set-up to provide improved accuracy. Examples of such studies are available in [32].

There are a series of improvements to the current model that need to be further explored, such as the ModClark transformation method was available only for grid cells that were at least $400 \text{ m} \times 400 \text{ m}$ (hence the selection of $500 \text{ m} \times 500 \text{ m}$ resolution) and the time step could be reduced from one day to a smaller one, provided that precipitation data is available on a smaller time step.

Regular update of landcover products is important [33,34] but challenging for physical process-based models [35] and is not commonly carried out. Further research into LULC automatic updates and their inclusion in the model along with climate change scenarios would give further insights on the catchment response.

Author Contributions: Conceptualization and methodology, P.P., T.H.A., A.J. and I.P.; data curation, investigation and formal analysis, P.P.; writing—original draft preparation, P.P.; writing—review and editing, T.H.A., A.J. and I.P.; supervision, T.H.A., A.J. and I.P. All authors have read and agreed to the published version of the manuscript.

Funding: This research received no external funding.

Data Availability Statement: The data presented in this study are available on request from the corresponding author. The data are not publicly available, as they are property of different Scent stakeholders.

Acknowledgments: The authors are thankful to all volunteers that participated in the Scent Project and the support of the Scent Project in providing data (grant agreement No. 688930).

Conflicts of Interest: The authors declare no conflicts of interest.

References

- Zhang, C.; Takase, K.; Oue, H.; Ebisu, N.; Yan, H. Effects of land use change on hydrological cycle from forest to upland field in a catchment, Japan. *Front. Struct. Civ. Eng.* **2013**, *7*, 456–465. [\[CrossRef\]](#)
- Berihun, M.L.; Tsunekawa, A.; Haregeweyn, N.; Meshesha, D.T.; Adgo, E.; Tsubo, M.; Masunaga, T.; Fenta, A.A.; Sultan, D.; Yibeltal, M.; et al. Hydrological responses to land use/land cover change and climate variability in contrasting agro-ecological environments of the Upper Blue Nile basin, Ethiopia. *Sci. Total Environ.* **2019**, *689*, 347–365. [\[CrossRef\]](#) [\[PubMed\]](#)
- Jacobs, J. Flood List. Report—Flood Losses in Europe to Increase Fivefold by 2050, 17 February 2016. Available online: <http://floodlist.com/europe/report-floods-europe-increase-fivefold-2050> (accessed on 19 May 2020).
- United Nations. The speed of urbanization around the world. *Dep. Econ. Soc. Aff. Popul. Div.* **2018**, *2018/1*, 2.
- Adams, M.; Lükewille, A. *The European Environment-State and Outlook European Environment Agency*; Publications Office of the European Union: Luxembourg, 2010; p. 4.
- Wickramarachchi, C.; Popescu, I.; Jonoski, A.; Wenninger, J. Use of globally available data for determining water level variation in lakes: The case study of Lake Turkana, Kenya. *Geoecomarina J.* **2023**, *29*, 169–186. [\[CrossRef\]](#)
- de Sherbinin, A.; Bowser, A.; Chuang, T.R.; Cooper, C.; Danielsen, F.; Edmunds, R.; Elias, P.; Faustman, E.; Hultquist, C.; Mondardini, R.; et al. The Critical Importance of Citizen Science Data. *Front. Clim.* **2021**, *3*, 20. [\[CrossRef\]](#)
- Baxevanis, J. Population, internal migration and urbanization in Greece. *Balk. Stud.* **1965**, *6*, 83–98.
- Plecher, H. Greece: Degree of Urbanization from 2008 to 2018. 2020. Available online: <https://www.statista.com/statistics/276402/urbanization-in-greece/> (accessed on 19 May 2020).
- Strobl, B.; Etter, S.; van Meerveld, I.; Seibert, J. Accuracy of crowdsourced streamflow and stream level class estimates. *Hydrol. Sci. J.* **2019**, *65*, 823–841. [\[CrossRef\]](#)
- Assumpção, T.H.; Jonoski, A.; Theona, I.; Tsiakos, C.; Krommyda, M.; Tamascelli, S.; Kallioras, A.; Mierla, M.; Georgiou, H.V.; Miska, M.; et al. Citizens' Campaigns for Environmental Water Monitoring: Lessons from Field Experiments. *IEEE Access* **2019**, *7*, 134601–134620. [\[CrossRef\]](#)
- Diakakis, M.; Deligiannakis, G.; Pallikarakis, A.; Skordoulis, M. Factors controlling the spatial distribution of flash flooding in the complex environment of a metropolitan urban area. The case of Athens 2013 flash flood event. *Int. J. Disaster Risk Reduct.* **2016**, *18*, 171–180. [\[CrossRef\]](#)
- Athens Population. 2020. Available online: <http://worldpopulationreview.com/world-cities/athens-population/> (accessed on 19 May 2020).
- Mimikou, M.; Baltas, E. A study of extreme storm events in the Greater. In *The Extremes of the Extremes: Extraordinary Floods*; International Association of Hydrological Sciences: Wallingford, UK, 2002; p. 161.
- Mazi, K.; Koussis, A. The 8 July 2002 storm over Athens: Analysis of the Kifissos River/Canal overflows. *Adv. Geosci.* **2006**, *7*, 301–306. [\[CrossRef\]](#)
- Bathrellos, G.; Karymbalis, E.; Skilodimou, H.; Gaki-Papanastassiou, K.; Baltas, E. Urban flood hazard assessment in the basin of Athens Metropolitan city, Greece. *Environ. Earth Sci.* **2016**, *75*, 319. [\[CrossRef\]](#)
- Chrysoulakis, N.; Mitiraka, Z.; Stathopoulou, M.; Cartalis, C. A comparative analysis of the urban web of the greater Athens agglomeration for the last 20 years period on the basis of Landsat imagery. *Fresenius Environ. Bull.* **2013**, *22*, 2139–2144.
- Marsalek, J.; Watt, W.E.; Zeman, E.; Sieker, H. *Advances in Urban Stormwater and Agricultural Runoff Source Controls*; Springer Science & Business Media: Berlin/Heidelberg, Germany; IOS Press: Amsterdam, The Netherlands, 2012; pp. 140–143.
- Sahu, M.K.; Shwetha, H.R.; Dwarakish, G.S. State-of-the-art hydrological models and application of the HEC-HMS model: A review. *Model. Earth Syst. Environ.* **2023**, *9*, 3029–3051. [\[CrossRef\]](#)
- Gitas, I. Copernicus Land Monitoring Service. 10442/15383. 2016; Volume 34, p. 56. Available online: <https://land.copernicus.eu/en> (accessed on 10 September 2024).
- USACE. *Hydrologic Modeling System HEC-HMS Applications Guide*; Hydrologic Engineering Center: Davis, CA, USA, 2002.
- Panagos, P. The European soil database. *GeoConnex* **2006**, *5*, 32–33.
- Tegos, A.; Mamassis, N.; Koutsoyiannis, D. Estimation of potential evapotranspiration with minimal data dependence. In *EGU General Assembly Conference Abstracts*; European Geosciences Union: Vienna, Austria, 2009.
- Ali, M.H. *Framework for Improving Flood Models by Integrating Crowdsourced Data in the Poorly Gauged Catchment of Kifissos, Greece*; UNESCO-IHE: Delft, The Netherlands, 2018.
- Verbeiren, B.; Khanh Nguyen, H.; Wirion, C.; Batelaan, O. An Earth observation based method to assess the influence of seasonal dynamics of canopy interception storage on the urban water balance. *Belgeo. Rev. Belg. Géographie* **2016**, *6*. [\[CrossRef\]](#)
- Nistor, M.-M.; Man, T.C.; Benzaghta, M.A.; Nedumpallile Vasu, N.; Dezsí, S.; Kizza, R. Land cover and temperature implications for the seasonal evapotranspiration in Europe. *Geogr. Tech.* **2018**, *13*, 90–91. [\[CrossRef\]](#)
- Bennett, T.H. *Development and Application of a Continuous Soil Moisture Accounting Algorithm for the Hydrologic Engineering Center Hydrologic Modeling System (HEC-HUMS)*; University of California: Davis, CA, USA, 1998.
- Feldman, A.D. *Hydrologic Modeling System HEC-HMS: Technical Reference Manual*; US Army Corps of Engineers, Hydrologic Engineering Center: Davis, CA, USA, 2000; pp. 123–126.
- Tilley, J.S.; Slonecker, E.T. *Quantifying the Components of Impervious Surfaces*; Open-File Report 2006; U.S. Geological Survey: Reston, VA, USA, 2006; pp. 17–18.

30. El-Nesr, M.N. Subsurface Drip Irrigation System Development and Modeling of Wetting Pattern Distribution. Ph.D. Thesis, Alexandria University, Alexandria, Egypt, 2006.
31. Woodward, D. *Part 630 Hydrology National Engineering Handbook-Chapter 15 Time of Concentration*; United States Department of Agriculture: Washington, DC, USA, 2010; p. 15-3.
32. Reddy, B.S.N.; Pramada, S.K. A hybrid artificial intelligence and semi-distributed model for runoff prediction. *Water Supply* **2022**, *22*, 6181. [[CrossRef](#)]
33. Chirachawala, C.; Shrestha, S.; Babel, M.S.; Viridis, S.G.P.; Wichakul, S. Evaluation of global land use/land cover products for hydrologic simulation in the Upper Yom River Basin, Thailand. *Sci. Total Environ.* **2020**, *708*, 135148. [[CrossRef](#)] [[PubMed](#)]
34. Chaves, M.E.D.; Picoli, M.C.A.; Sanches, I.D. Recent applications of Landsat 8/OLI and Sentinel-2/MSI for land use and land cover mapping: A systematic review. *Remote Sens.* **2020**, *12*, 3062. [[CrossRef](#)]
35. Brunner, M.I.; Slater, L.; Tallaksen, L.M.; Clark, M. Challenges in modeling and predicting floods and droughts: A review. *WIREs Water* **2021**, *8*, e1520. [[CrossRef](#)]

Disclaimer/Publisher’s Note: The statements, opinions and data contained in all publications are solely those of the individual author(s) and contributor(s) and not of MDPI and/or the editor(s). MDPI and/or the editor(s) disclaim responsibility for any injury to people or property resulting from any ideas, methods, instructions or products referred to in the content.